Microscopic structure of liquid hydrogen

2003 J. Phys.: Condens. Matter 15 R1047

(http://iopscience.iop.org/0953-8984/15/23/202)

INSTITUTE OF PHYSICS PUBLISHING JOURNAL OF PHYSICS: CONDENSED MATTER

J. Phys.: Condens. Matter **15** (2003) R1047–R1062 PII: S0953-8984(03)56287-7

TOPICAL REVIEW

Microscopic structure of liquid hydrogen

Marco Zoppi

Consiglio Nazionale delle Ricerche, Istituto di Fisica Applicata 'Nello Carrara',
Via Panciatichi 56/30, I-50127 Firenze, Italy

E-mail: zoppi@ifac.cnr.it

Received 9 April 2003
Published 30 May 2003
Online at stacks.iop.org/JPhysCM/15/R1047

Abstract

Hydrogen makes the simplest molecular liquid. Nonetheless, due to several different reasons, measuring its microscopic structure has been one of the most challenging tasks in neutron diffraction experiments. The recent development of modern pulsed neutron sources triggered a renewed experimental interest which, in turn, led to new knowledge and also to a more effective use of the classic reactor-based experimental data. The contemporary development of quantum mechanical computer simulation techniques, and a critical comparison among the results of different experiments using steady and pulsed neutron sources, resulted in a quantitatively reliable solution of the problem.

Contents

1. Introduction

Hydrogen is the most abundant element in the universe and the third most abundant element on earth's surface (after oxygen and silicon). The hydrogen molecule, a homonuclear diatomic molecule composed of two protons 74 pm apart and two electrons, is probably the most deeply

Table 1. Fixed points properties of hydrogen isotopes in normal composition [10]. The labels CP and TP indicate the triple point and the critical point, respectively. The density n_{TP} refers to the liquid phase. The critical parameters of tritium are estimated.

	T_{CP} (K)	p_{CP} (bar)	n_{CP} (nm^{-3})	T_{TP} (K)	p_{TP} (bar)	n_{TP} (nm^{-3})
Hydrogen	33.19	13.15	9.00	13.96	0.072	23.06
Deuterium	38.34	16.65	10.44	18.71	0.171	26.00
Tritium	40.44	18.50	10.88	20.62	0.216	27.33

studied. Hydrogen was first liquefied in 1898 by Dewar, but observation of mist and liquid droplets dates back to 1877 [1]. Mecke [2] spectroscopically detected two different species of hydrogen in 1924 and Heisenberg in 1926, [3], gave the quantum mechanical interpretation that subsequently led to the definition of ortho- and para-hydrogen. The discovery of hydrogen isotopes is relatively recent. Deuterium was spectroscopically detected, as an impurity of hydrogen, by Urey *et al* [4] in 1932, while Oliphant *et al* [5] first made tritium, in 1934, from deuterium nuclear collisions. Tritium was found to be radioactive by Alvarez and Cornog in 1939 [6]. Its presence was detected in atmospheric hydrogen by Faltings and Harteck [7] in 1950, and in rainwater by Libby *et al* [8] in 1951.

The thermodynamic fixed points of the hydrogen isotopes in normal composition (i.e. that corresponding to the room-temperature thermodynamic equilibrium between the ortho- and the para-species) are shown in table 1. A rather large isotopic effect emerges immediately. However, since the electronic cloud distribution is not expected to change substantially from one isotope to the other, it is not unreasonable to assume that the three isotopes experience the same intermolecular potential [9]. Thus, the observed variance in the thermodynamic behaviour should be mostly attributed to the change in molecular mass which, in turn, determines the size of the quantum effects.

Quantum effects in condensed matter originate from the delocalization of particles whose centre of mass (COM) cannot be associated with individual points in space but, more properly, to a probability distribution [11]. The width of this space distribution is somehow related to the de Broglie (DB) thermal wavelength, λ_{DB}, which depends on the mass of the particle and on the temperature, according to the definition [12]

$$\lambda_{DB} = \hbar/(2\pi M k_B T)^{1/2} \tag{1}$$

where $\hbar$ is the Planck constant, M is the mass, T is the temperature and k_B is the Boltzmann constant. Strictly speaking, the definition of λ_{DB} only applies to a free particle and a different definition should be used when a set of interacting particles is considered. However, this difference is not expected to change substantially the following qualitative considerations.

At the classical limit ($T \to \infty$) λ_{DB} vanishes identically. At finite temperatures, λ_{DB} grows by decreasing temperature until it becomes appreciable. The DB wavelength can be compared with an intramolecular length scale (e.g. σ_{HC}, the hard-core diameter) or with an intermolecular length scale (e.g. ℓ the nearest neighbour distance). Initially, λ_{DB} becomes sizeable with respect to σ_{HC}. This is the region where quantum diffraction effects start to play a role but the single particles still retain their individuality and Boltzmann statistics (distinguishable particles) apply. By further decreasing the temperature, the width of the single-particle probability distribution grows more and more until it becomes so large that the wavefunction tails of neighbouring particles begin to overlap. In this case, quantum exchange becomes effective and particles lose their individuality. Depending on the spin of the particles, Fermi–Dirac or Bose–Einstein quantum statistics apply and very peculiar macroscopic effects emerge like, for example, superconductivity in the electron gas of metals or superfluidity in liquid ^{4}He.

Para-hydrogen is the most stable form of molecular hydrogen at low temperature. Here, the two protons exhibit an antiparallel spin configuration. Thus, the total nuclear spin vanishes identically and the molecule, in its fundamental state, appears quite similar to helium. However, in spite of the lower molecular mass, no effect driven by quantum exchange has ever been observed in bulk liquid hydrogen. In fact, due to a deeper intermolecular potential well, hydrogen becomes solid at a temperature higher than helium[1]. Hence, the DB wavelength of bulk liquid hydrogen is never allowed to become comparable to that of helium close to the λ-transition.

Fluid hydrogen occupies an extremely relevant position in technological and scientific applications. Dense supercritical hydrogen was widely used to make bubble chambers [13, 14]. In addition, due to their light nuclear mass, hydrogen nuclei are used to slow down fast neutrons [15]. This has important consequences in neutron physics, where hydrogen moderators are used to produce cold neutrons for spectroscopic applications [15]. Liquid hydrogen was used as a cryogenic refrigerant before liquid helium, or in any case when a higher boiling point refrigerant was required. Also, liquid hydrogen is a common, highly energetic rocket fuel and, in recent times, has been also proposed as a clean energy supply for automotive transportation [16]. For these reasons, the thermodynamics of condensed hydrogen has been extensively studied. However, not much was known about its microscopic structure until recently.

2. Measuring the microscopic structure of a liquid

In condensed matter, typical intermolecular distances are of the order of a few angstroms. In principle, this range of distances is efficiently probed by diffraction techniques using either x-rays or thermal neutrons. In the old days, x-ray diffraction techniques were mostly applied to measure the microscopic structure factor of simple liquids [17]. However, neutron techniques were growing fast [18] and their powerful potential was shown in a celebrated experiment by Yarnell *et al* [19] on liquid argon. Since then, neutron diffraction experiments have been widely used to determine the microscopic structure factor of simple (and not so simple) liquids [20, 21]. However, no reliable experimental determination of the microscopic structure of liquid hydrogen was available in 1991 [22].

In practice, there are experimental difficulties in applying x-ray or neutron diffraction techniques to a liquid hydrogen sample. On the one hand, the small number of electrons makes hydrogen almost transparent to x-rays. On the other hand, neutron diffraction reveals difficulties too. In either case, the scattering event is assumed to be elastic, i.e. the momentum–energy loss from the probe to the target is assumed to be negligible. This is a well-satisfied condition in x-ray scattering [11], provided Compton scattering is neglected. However, in neutron scattering, this condition only applies when the mass of the probe is negligible with respect to the effective mass of the target nucleus. If this assumption is not satisfied, as in hydrogen, the target nucleus undergoes a substantial recoil with a consequent loss of the neutron energy. This implies that the neutron diffraction data are strongly affected by inelasticity effects. The usual correction technique, known as Placzek correction [23], is based on a perturbative expansion in terms of the mass ratio between the neutron and the target nucleus. Obviously, such a correction procedure is not expected to converge when applied to hydrogen, where the mass ratio is $\simeq 1$.

Along with this problem, there is a second drawback when dealing with neutron scattering on hydrogen. In fact, the interaction between the neutron probe and the target nucleus is ruled

[1] As the system becomes solid, each molecule sits in the potential well produced by the cage of neighbours. This makes the particle wavepackets more localized and the overlap negligible.

by the Fermi pseudo-potential [24]. This, in turn, contains a complex (i.e. composed of a real and imaginary part) scattering length which is determined by the specific spin transition occurring during the scattering event [25, 26]. When no spin transition occurs, then the neutron retains its phase coherence. Thus, scattering events pertaining to neighbouring nuclei give rise to interference effects (coherent neutron scattering) which, in turn, carry information on the local structure surrounding the target particle. On the contrary, when a spin transition occurs, a random phase factor appears in the scattering cross sections which wipes out any possible spatial interference among local neighbours (incoherent neutron scattering). For hydrogen, it turns out that the incoherent scattering cross section is almost two orders of magnitude larger than the coherent one. Therefore, the coherent signal, which carries information on the microscopic local structure of liquid hydrogen, is expected to be extremely small with respect to a large incoherent background. This explains why no generally accepted experimental structure factor determination of liquid hydrogen was available until recently.

It is important to note that, concerning the neutron diffraction experiments, there is a substantial difference between hydrogen and deuterium. In fact, for the heavier isotope, the coherent and incoherent scattering cross sections turn out to be of comparable size. Moreover, because of the larger mass, the evaluation of the recoil corrections is less demanding. Therefore, in deuterium, the signal carrying the structural information lies on top of a background of a similar magnitude.

3. Basic scenario of a neutron diffraction experiment

3.1. The experimental side

Essentially, there are two ways of performing a neutron diffraction experiment. In the first one, a steady neutron source is used (e.g. a nuclear reactor), and the incident neutron beam is selected within a narrow energy window. The secondary flux, i.e. that scattered by the sample, is collected by a suitable detector placed at a certain scattering angle. By assuming that the scattering is elastic, and using the momentum conservation law, the momentum transfer $\hbar Q$ is determined by the scattering angle, θ, and the wavevector of the incident neutron, k_0, according to [26]

$$Q = 2k_0 \sin(\theta/2) \tag{2}$$

where $k_0 = 2\pi/\lambda_0$ and λ_0 is the wavelength of the neutron. The neutron energy is $E_0 = (\hbar k_0)^2/(2m)$ while m is the mass of the neutron. Since the energy of the incident neutrons is fixed, the only way of changing the momentum transfer, $\hbar Q$, is by changing the scattering angle θ.

For a monatomic liquid, the differential scattering cross section is given by [26]

$$\frac{\mathrm{d}\sigma}{\mathrm{d}\Omega} = (1/4\pi)\{\sigma_{coh}[S(Q) - 1] + \sigma_{tot}\} + P(Q) \tag{3}$$

where $\mathrm{d}\sigma/\mathrm{d}\Omega$ is the scattering cross section per unit solid angle, $S(Q)$ is the microscopic structure factor, $\sigma_{tot} = \sigma_{coh} + \sigma_{inc}$, while σ_{coh} and σ_{inc} are the *bound-nucleus* cross sections for the coherent and incoherent scattering, respectively. The additive term $P(Q)$ accounts for the inelastic scattering corrections (e.g. Placzek) and should be independently evaluated. From textbooks on scattering theory, it is known that the recoil effects that are accounted for by the correction term $P(Q)$ increase with the scattering angle. Therefore, if the experiment is carried out as outlined above, the size of the correction is expected to increase (as it does) with the value of Q.

As was anticipated, there is another way of performing a neutron diffraction experiment. Here, the probe comprises the white beam of a pulsed neutron source and the scattering angle

is kept fixed. Thus, using incident neutrons of different energies (i.e. different wavelengths) it is possible to span the momentum transfer over a rather large interval (cf equation (2)) without changing the scattering angle. The energy (and wavelength) of the neutrons is measured using a time-of-flight (TOF) technique. In principle, by selecting the scattering angle at a sufficiently low value, the inelasticity recoil effects can be reduced below any preselected limit value. Taking advantage of these considerations, the first reliable neutron diffraction experiment on supercritical deuterium was carried out in 1988 on the liquid and amorphous diffractometer (LAD) at ISIS (UK) [27, 28]. The SANDALS (Small Angle Neutron Diffractometer for Amorphous and Liquid Samples) instrument was built at ISIS to exploit these features, i.e. a reduction of the inelastic correction terms using relatively small scattering angles [29]. This diffractometer was used to measure the microscopic structure factor of liquid deuterium close to the triple point [30] and in the compressed liquid phase along the melting line [31].

3.2. Understanding the neutron diffraction data

The interpretation of the neutron diffraction data for a homonuclear diatomic molecular system is slightly more complex than for the monatomic one. In fact, the measured cross section is determined by the correlations between pairs of nuclei which may, or may not, belong to the same molecule. In practice, the measured cross section is determined by the site–site correlation function which, in turn, is driven by the relevant *inter*- and *intra*-molecular dynamics. If we take into account that hydrogen behaves as an almost-free rotor, even in the solid phase [32], then we may assume, *a fortiori*, that the same situation applies to a fluid sample of hydrogen or deuterium. Therefore, it is reasonable to assume that the rotational and translational dynamics are not correlated [33]. Within this approximation, the expression for the cross section becomes [34]

$$\frac{\mathrm{d}\sigma}{\mathrm{d}\Omega} = u(Q)[S(Q) - 1] + v(Q) + P(Q) \tag{4}$$

where $S(Q)$ is the intermolecular COM static structure factor and the two functions $u(Q)$ and $v(Q)$ are molecular form factors which are interpreted as the *inter*- and *intra*-molecular neutron cross section, respectively. Again, $P(Q)$ accounts, in an effective way, for the inelastic scattering corrections. Its effect is shown to become less and less important as lower and lower scattering angles are used [27, 28].

To a first approximation, the two molecular form factors can be evaluated by assuming a rigid-rotor molecular model. In this case [34]

$$u(Q) = 4a_{coh}^2\,[\sin(Qd/2)/(Qd/2)]^2 \tag{5}$$

$$v(Q) = 2(a_{coh}^2 + a_{inc}^2) + B(I, X^{(o)})\,[\sin(Qd)/(Qd)] \tag{6}$$

where d is the bond length (internuclear distance), a_{coh} and a_{inc} are the coherent and incoherent scattering lengths of the nucleus, I is the nuclear spin, $X^{(o)}$ is the fraction of molecules in the *odd* state and $B(\cdot)$ is a suitable analytic function (e.g. see equations (9) and (10), below).

4. Neutron diffraction experiments on liquid deuterium

To our knowledge, the first report of a neutron diffraction experiment on liquid deuterium dates back to 1968 [35]. This pioneering task was carried out using neutrons of wavelength $\lambda = 1$ Å from a reactor source. However, the data turned out of a poor quality and little physical information could be obtained, as far as the intermolecular structure factor was concerned. A second experiment was carried out 20 years later by Ishmaev *et al* [36] using a pulsed neutron

source. The data appear to be of a better statistical quality and all the main qualitative features of the deuterium diffraction pattern are present. However, the need to sum the results of all the scattering angles between 22° and 135°, and the simple use of the Placzek procedure [23] to account for the inelastic corrections, made the results less than rigorous and the reported structure factor quantitatively incorrect [28].

As anticipated above, the first quantitatively reliable TOF neutron diffraction experiment in the fluid phase was carried out on supercritical deuterium using the LAD at ISIS [27]. Here, by means of a direct inversion procedure, the site–site radial distribution function was derived which shows a characteristic intramolecular peak at $\simeq 0.75$ Å. An intermolecular structure was also observed at higher radial distance. This was compared with a classical Monte Carlo (MC) simulation [37] for a monatomic system of mass $M = 4$ au, interacting through a Lennard-Jones potential. The intermolecular structure factor from the simulation data was interpreted as the COM $S(Q)$ and the rigid-rotor model (equation (4)) was used to evaluate the site–site theoretical cross section. This was found to be in semi-quantitative agreement with the experiment [27]. In a subsequent paper [38] the same experimental data were compared with the results of a quantum path integral Monte Carlo (PIMC) simulation [39] using the same free-rotor approximation. Excellent overall agreement was found (cf figure 7 of [38]) but the high value of the reduced χ^2 called for improvements both in experimental accuracy and in the theoretical model.

The next experiment was performed on the newly built SANDALS diffractometer at ISIS. The measurements were carried out in liquid deuterium close to the triple point. Five thermodynamic points were selected, three on the same isotherm and three on the same isochore. Therefore, not only the structure factor, but also its thermodynamic derivatives could be evaluated [30]. In this experiment, the improved instrument efficiency at small scattering angles was exploited, and provided evidence on the limitations of the free-rotor model. In fact, more accurate modelling of the molecular structure was required. An obvious generalization was attempted, taking into account the zero-point motion of the vibrational ground state and introducing a Debye–Waller factor. However, this simple model did not produce a satisfactory fit to the experimental data that were suggesting a slight change in the molecular parameters [30].

An improved dynamic model for molecular hydrogen, in the diluted gas phase, had been proposed by Young and Koppel (YK) [40]. Here, the hydrogen molecule was modelled as a freely rotating harmonic oscillator but no intermolecular interaction was accounted for. A modified Young and Koppel (MYK) model was developed which included an effective isotropic intermolecular interaction [41]. Within this model, the *inter*- and the *intra*-molecular cross sections $u(Q)$ and $v(Q)$, respectively, were calculated exactly. It turns out [41] that the rigorous analytic solution for these two functions can be very well approximated by the solution of a zeroth-order approximation (rigid-rotor term modulated by a Debye–Waller factor), provided the true molecular parameters are replaced by the effective ones. In conclusion, the expressions for the *inter*- and the *intra*-molecular cross section become

$$u(Q) = 4a_{coh}^2\,[\exp(-\lambda_{DW}^2 Q^2/2)\sin(Qd/2)/(Qd/2)]^2 \tag{7}$$

$$v(Q) = 2(a_{coh}^2 + a_{inc}^2) + B(I, X^{(o)})\,\exp(-2\lambda_{DW}^2 Q^2)\sin(Qd)/(Qd) \tag{8}$$

where the molecular parameters, λ_{DW} and d, assume effective values that are not much different from the respective true values. It is important to stress, once more, that the function $B(I, X^{(o)})$ depends on the spin of the nucleus and on the relative concentration of the molecules in the *odd* or *even* state [41]. For deuterium, $I = 1$ and the expression for $B(I, X^{(o)})$ is

$$B_D(X^{(o)}) = B(1, X^{(o)}) = 2a_{coh}^2 - \tfrac{1}{2}a_{inc}^2[3X^{(o)} - 1], \tag{9}$$

Table 2. True and effective (calculated) molecular parameters for hydrogen and deuterium. (Due to a misprint in the caption, the values reported in table 1 of [41] are incorrect by a factor of 2. In addition, the present values have been recalculated using a more accurate value for the first vibrational energy transition $E_v(\mathrm{H}) = 0.5159$ eV and $E_v(\mathrm{D}) = 0.3712$ eV.) The internuclear distance is d and the Debye–Waller *length factor* is λ_{DW}. This is defined as $\lambda_{DW} = (\hbar/2M\omega_v)^{1/2}$, where M is the molecular mass and ω_v is the vibrational angular frequency (rad s^{-1}).

	Hydrogen		Deuterium	
	True	Effective	True	Effective
λ_{DW} (nm)	0.4483	0.4517	0.3739	0.3759
d (nm)	7.414	7.303	7.415	7.338

while for hydrogen, $I = \frac{1}{2}$ and

$$B_H(X^{(o)}) = B(\tfrac{1}{2}, X^{(o)}) = 2a_{coh}^2 - 2a_{inc}^2[1 - \tfrac{4}{3}X^{(o)}]. \tag{10}$$

It is worth noticing that in the high-temperature limit, i.e. when the normal *ortho–para* concentration is realized, the dependence on $X^{(o)}$ disappears and the two expressions reduce to the same form:

$$B_{normal} = 2a_{coh}^2. \tag{11}$$

The comparison between the true and effective (calculated) molecular parameters for hydrogen and deuterium is reported in table 2. The model outlined above was used to analyse the TOF neutron data of liquid deuterium taken on SANDALS [30, 31].

Following the first TOF experiment [30], a second one was performed on a conventional two-axis diffractometer (7C2 at Laboratoire Léon Brillouin, CEA-Saclay, France) still on liquid deuterium and in similar thermodynamic conditions [42]. The rationale was that, using fixed-energy neutrons, the effect of the inelastic corrections could have been easily calculated, since only a few rotational and no vibrational transitions were excited by the relatively low-energy neutrons used in this experiment. A quantitative comparison between the two experiments was extremely positive [43], with somehow lower error bars in the reactor-based experimental data. The overall agreement between two independent experimental determinations of the structure factor of liquid deuterium, carried out using different instruments and techniques, was also emphasized by a quantitatively positive comparison with quantum mechanical PIMC simulation results [44].

5. Neutron diffraction experiments on liquid hydrogen

In spite of the successful results obtained on liquid deuterium, the experimental determination of the structure factor for liquid hydrogen still constitutes a formidable task. In practice, due to the presence of the incoherent scattering length in the expression for $v(Q)$ (cf equation (7)), the largest fraction of scattering power, for a hydrogen sample, is determined by the *intra*-molecular cross section. Therefore, any instrumental systematic uncertainty, though small, is likely to mask the coherent intramolecular term. Driven by this consideration, we resolved to perform a difference experiment on liquid hydrogen where the object of the investigation was not the microscopic structure factor, $S(Q)$, but its thermodynamic derivatives. In addition, using the results of the MYK model [41], and assuming that the COM structure factor of liquid hydrogen would be similar to that of deuterium, we could make a prediction of the expected diffraction pattern. Thus, we discovered that, in the calculated cross section, the expected ratio between the coherent contribution and the intramolecular background would improve from a

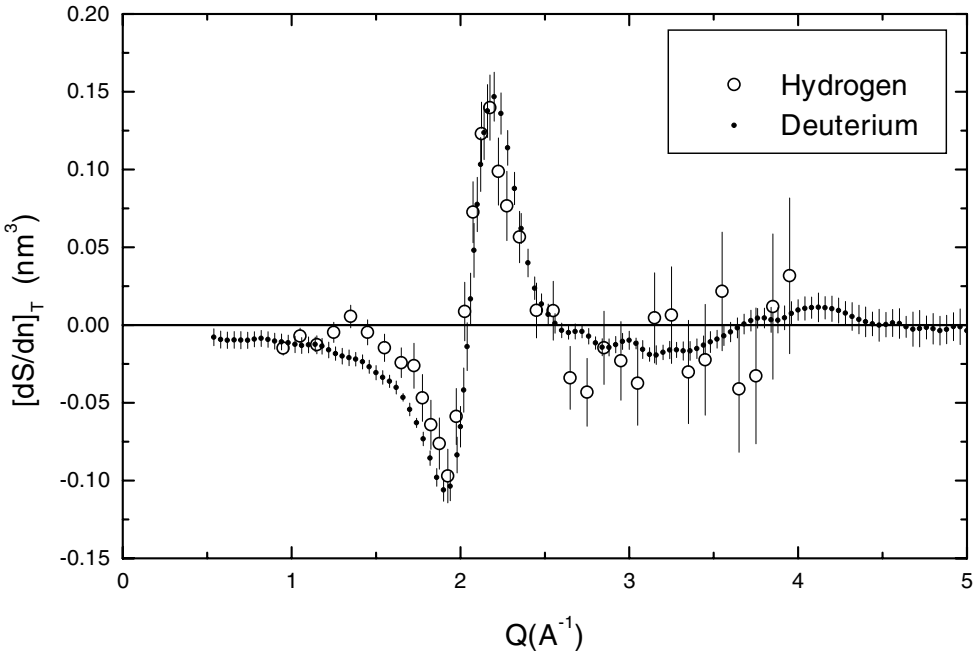

Figure 1. Experimental density derivative, at constant temperature, of the structure factor of liquid hydrogen. The open circles are the hydrogen data from [45] while the dots represent the deuterium data from [44].

level of 4% in normal hydrogen to a more appealing 10% in pure para-hydrogen. Again the experiment was carried out on the SANDALS diffractometer, measuring five thermodynamic points in the vicinity of the triple point in a sample of almost pure para-hydrogen [45].

The experimental data analysis showed that, even though it was not possible to extract reliable information on the microscopic structure factor, $S(Q)$, the thermodynamic derivatives could be obtained with a reasonable quantitative accuracy [45]. In figure 1 we show the resulting density-derivative of the intermolecular COM structure factor (open circles) for liquid para-hydrogen. The dots show the same quantity for liquid deuterium, under similar thermodynamic conditions [44]. Even though the error bars on the hydrogen data are generally relevant, two things emerge from the figure. The first is a steeper decrease at increasing Q-values and a narrower minimum. The second is that, in the region of the peak at $Q = 2.2$ Å^{-1}, the hydrogen data seem to be located systematically to the left of those of deuterium. Similar behaviour also emerges from the temperature derivative which is reported in figure 2. Again, the hydrogen data (open circles) appear systematically on the left with respect to deuterium (dots).

The observed effect has a simple, intuitive, explanation. Let us imagine plotting the same figures as a function of a reduced momentum transfer, $Q^\star = Q\sigma$, where σ is a molecular scale length that can be associated with an effective molecular size of the particular isotope. In order for the two systems (i.e. hydrogen and deuterium) to give an equivalent answer, we should allow for a hydrogen molecular diameter *larger* than that of deuterium. This is interpreted as a signature of the quantum effects which determine, in hydrogen, an effective molecular wavepacket slightly broader than that of deuterium, just because of the smaller molecular mass (cf equation (1)).

The reliability of the MYK model for liquid hydrogen was also tested in a subsequent transmission experiment, where the total cross section of liquid para-hydrogen was directly

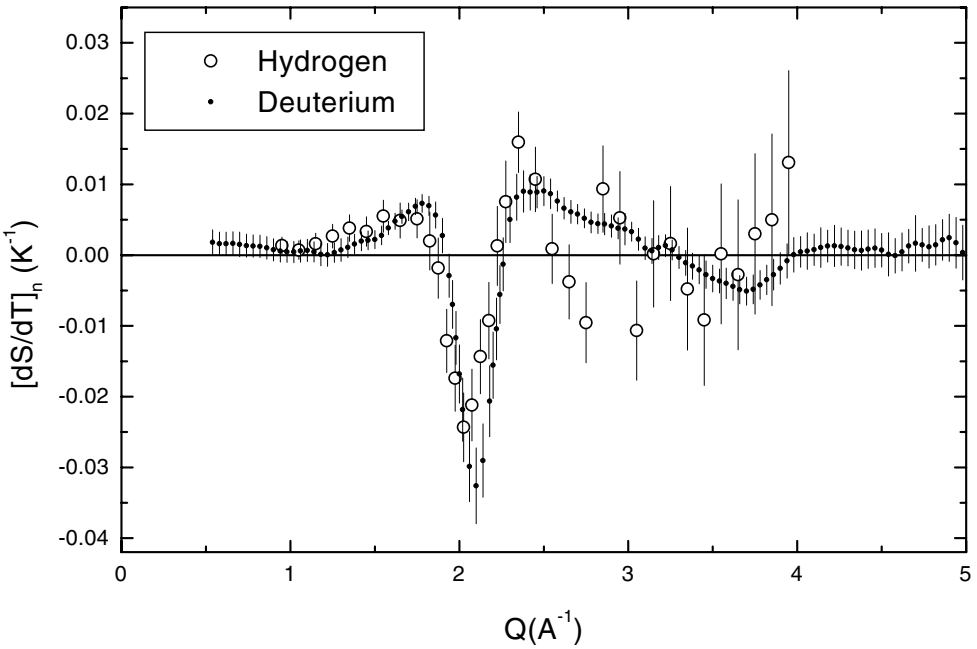

Figure 2. Experimental temperature derivative, at constant density, of the structure factor of liquid hydrogen. The open circles are the hydrogen data from [45] while the dots represent the deuterium data from [44].

measured as a function of the incident neutron energy [46]. Here, theory and experiment were found to be in a nice quantitative agreement by assuming for $\langle E_K \rangle$, the average COM translational kinetic energy of liquid hydrogen, a value larger than the classical one. This is a well-known effect among quantum systems. The average kinetic energy of liquid and solid hydrogen has been measured, using independent experiments, and was found to be always larger than the classical value and dependent on density [47–50].

The extended knowledge gained from the properties of liquid hydrogen permitted us to design a new neutron diffraction experiment on a standard reactor source. This experiment was carried out on the D4 diffractometer at ILL (Institute Laue-Langevin, Grenoble) and has allowed a reliable determination of $S(Q)$, the microscopic COM structure factor of liquid para-hydrogen [51]. This is shown in figure 3 (open circles), together with the experimental results of liquid deuterium (dots) taken from [44]. The error bars affecting the para-hydrogen data appear sensibly larger than those of deuterium, which hardly exceed the size of the dots in the figure. At any rate, as for the thermodynamic derivatives, the hydrogen structure factor appears shifted slightly to lower Q-values, which confirms a larger effective diameter for the hydrogen molecule with respect to deuterium.

6. Comparison with quantum mechanical simulation results

The experimental data described in the previous section have been compared with the results of several PIMC [39] simulations carried out under thermodynamic conditions similar to the experiments. For both hydrogen isotopes, the same intermolecular pair potential was used. This is the isotropic component of the phenomenological potential given by Norman, Watts and Buck (NWB) [52]. The simulations were generally carried out using $N = 500$ classical particles and several Trotter numbers (P = number of beads in the classical isomorphic

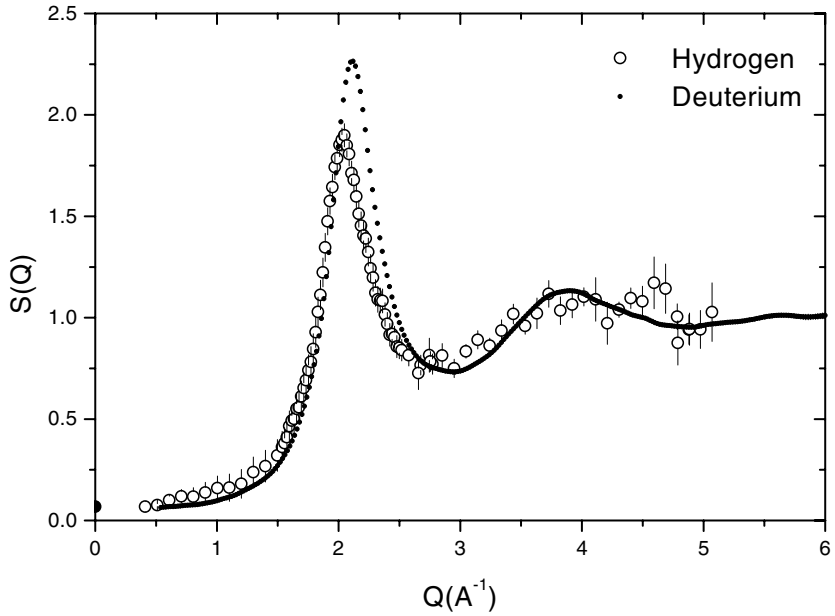

Figure 3. Intermolecular COM structure factor of liquid hydrogen. The open circles represent the para-hydrogen experimental data from [51] while the dots show the deuterium experimental data taken from [44].

polymer system). After a suitable number of equilibration moves, starting from a random initial configuration, the various stochastic configurations produced by the PIMC sequence are used to evaluate the thermodynamic averages. The PIMC results have been analysed as a function of P and it was found that $P = 16$ was sufficiently accurate for deuterium [38, 44], while $P = 32$ was sufficiently large to represent the correct quantum limit of hydrogen [53].

The particular choice of the intermolecular pair potential does not seem to play a very important role, as far as the qualitative features of the microscopic structure factor are concerned. However, quantitative differences can be evidenced, and were actually shown in [44], where $S(Q)$ and its thermodynamic derivatives were discussed for the case of liquid deuterium. In this case, the differences between the simple Lennard-Jones and the semi-empirical NWB potential were analysed and significant differences were observed. By contrast, when the comparison is carried out between two equally reliable interaction models, the resulting differences become much smaller and the possibility of selecting the best potential depends very much on the quality of the experimental data. This case was recently analysed by comparing the PIMC results using both the NWB and the SG (see [54]) potentials which, for hydrogen, give quantitatively equivalent results [53].

The limited number of particles ($N = 500$) is not large enough to produce a simulation $g(r)$ sufficiently extended in r to obtain a smooth $S(Q)$ by Fourier transformation. This is particularly visible in the deuterium data (cf figures 4 and 5) where the effect of the truncation errors appears as an oscillation in the simulation data, in particular at low Q-values. In order to reduce truncation errors, the cut-off radius should be extended from $\approx$14 Å (i.e. half the size of the simulation box) to a more suitable value of $\approx$30 Å. However, this would increase N by a factor of $\approx$10 and the CPU time by approximately two orders of magnitude. This would affect, in particular, the hydrogen simulations, due to the need to extend the Trotter number to 32. Thus, a different way of extending the range of $g(r)$ had to be devised in order to circumvent

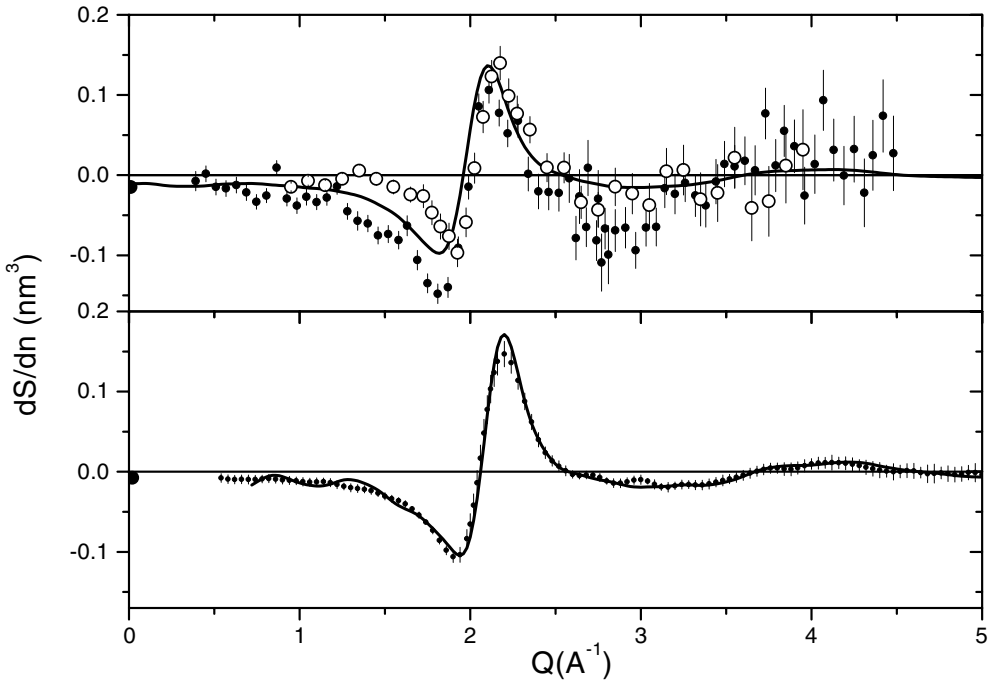

Figure 4. Density derivative of the COM structure factor of liquid hydrogens and their comparison with the PIMC simulation data (full curve). The upper figure refers to the liquid para-hydrogen. Here, the open circles represent the SANDALS experimental data from [45] while the dots are the D4 data from [51]. The PIMC simulation results are taken from [58]. In the lower figure (liquid deuterium), the dots are the experimental point and the line represents the PIMC results. Both are taken from [44]. In both figures, the large dot at $Q = 0$ represents the thermodynamic limit obtained from the experimental equation of state.

this limit. To this end, an extrapolation procedure suggested by Verlet [55] was applied to the hydrogen simulations. Following Verlet, the tails of the function $h(r) = g(r) - 1$ are extended by using a damped oscillating form:

$$h(r) = (A/r)\exp(-r/r_0)\sin(r/r_1), \tag{12}$$

where the parameters A, r_0 and r_1 are obtained by fitting the functional form (12) to the simulation results, starting from the third zero of $h(r)$.

In figure 4, the comparison between the experimental results and the PIMC simulations for the density derivative of the COM structure factor of the hydrogen is reported. We observe that, in the case of deuterium (lower figure), there is nice agreement, also quantitatively, between the PIMC calculations and the experimental results. For hydrogen, however, the agreement is less satisfactory (cf the upper figure 4). In the peak region of the density derivative, the two experimental data sets appear in almost quantitative agreement (within the error bars) and are substantially consistent with the PIMC simulation data. In the region of the minimum, however, the two data sets are at variance and the differences are larger than the reported experimental errors. This is likely indicative of some residual systematic error, still affecting one or both experiments, as seems to be testified by the PIMC simulation data that lie in between the two experimental data sets.

The temperature derivative of the COM structure factor, reported in figure 5, depicts a qualitatively similar behaviour. Again, the deuterium experimental data (lower figure) appear

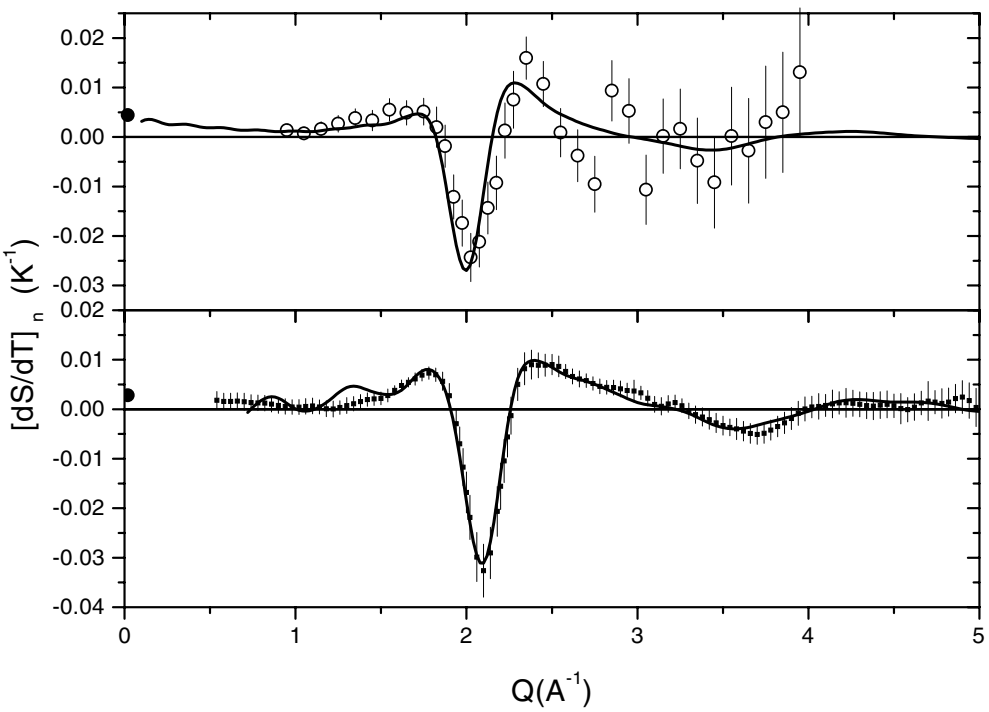

Figure 5. Temperature derivative of the COM structure factor of liquid hydrogen and its comparison with the PIMC simulation data (full curve). The upper figure refers to para-hydrogen. Here, the open circles represent the SANDALS experimental data from [45]. The PIMC simulation results are taken from [58]. The deuterium data are reported in the lower figure. Here the experimental and simulation data are taken from [44]. In both figures, the large dot at $Q = 0$ represents the thermodynamic limit obtained from the experimental equation of state.

in very good agreement with the PIMC simulation results (apart from some spurious oscillations at low Q produced by the truncation effects in the simulated $g(r)$), while some mismatch in the Q-scale is observed for the hydrogen data (upper figure). It is interesting to observe that, should the experimental hydrogen data agree with their PIMC simulations, this would increase the Q-scale mismatch, already observed in figure 2, between the deuterium and hydrogen experimental data.

7. Comparison with other experimental results

As discussed in the previous sections, a neutron diffraction experiment aiming to measure directly the structure factor of liquid hydrogen is not an easy task. In order to circumvent these problems, a different approach was recently attempted by Bermejo and co-workers [56], still using neutron scattering. Here, the main experimental objective appears to be the measurement of the dynamic structure factor, $S(Q, \omega)$, of liquid para-hydrogen that is accessed by means of an inelastic neutron scattering measurement. Then, the static structure factor, $S(Q)$, is derived taking advantage of the sum rule [26]:

$$S(Q) = \int_{-\infty}^{+\infty} \mathrm{d}\omega \, S(Q, \omega). \tag{13}$$

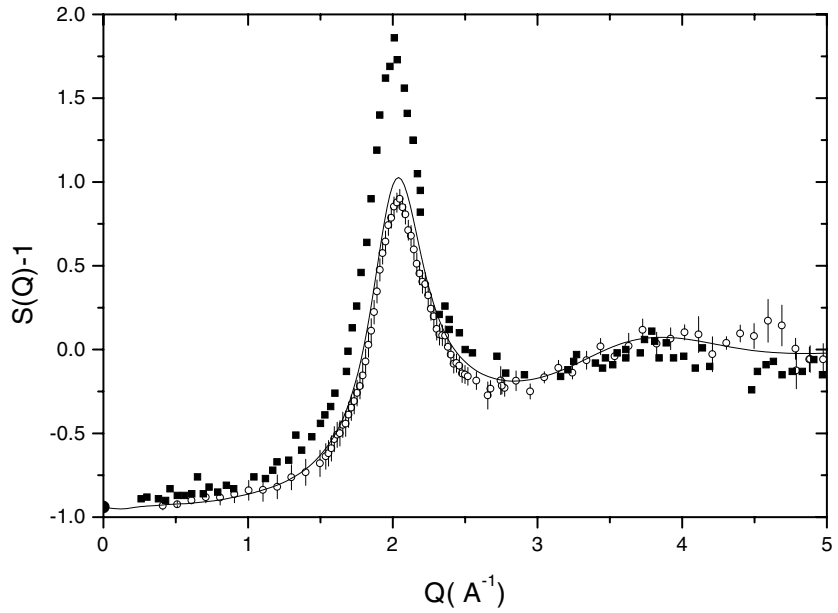

Figure 6. Comparison between two different neutron scattering experimental determinations of the COM structure factor of liquid para-hydrogen and the PIMC simulation results. The open circles are the diffraction data from [51] while the squares represent the data taken from figure 1 of [56]. The full curve is the PIMC simulation result, under similar thermodynamic conditions, as reported in [53].

The results of this procedure, however, are at variance with respect to the hydrogen data shown above. The most striking difference between the two experimental findings resides in the height of the main peak of $S(Q)$ which, as reported in figure 1 of [56], turns out much larger than in figure 3.

Even though it is not easy to assess two competing experimental techniques which give rather different results, there are a few circumstances that make the diffraction data, shown in figure 3, more appealing. First, the main peak of $S(Q)$, as reported in figure 1 of [56], exceeds the value of 2.85 that was defined by Hansen and Verlet [57] as corresponding to the onset of the freezing transition for a Lennard-Jones liquid. Even though the Hansen–Verlet criterion was formulated for a simple model system (classical monatomic particles interacting through a Lennard-Jones potential) it is hard to believe that $S(Q)$ for hydrogen, a genuine quantum system for which one expects a general broadening and damping of the structural features, should reach such a large value in the liquid phase. Second, the quantum mechanical PIMC simulation results do agree much better with the diffraction experimental data. The situation is depicted in figure 6.

One may argue that, in the end, the preference for the neutron diffraction data is based only on consistency with some simulation results, while this preference should be based more on solid experimental facts. However, there are more experimental data that may corroborate this preference. Recent x-ray experiments have been carried out at ESRF, the European Synchrotron Radiation Facility (Grenoble, France), using the same method described above, i.e. integrating the dynamic structure factor at constant Q, to determine the microscopic structure factor. The first experiment was carried out in compressed liquid hydrogen close to the critical temperature, i.e. at $T = 31.5$ K, at a density of $n = 21.5\ \mathrm{nm}^{-3}$ by Pratesi *et al* [59]. The second experiment

was carried out at a similar density, $n = 21.24$ nm^{-3}, but at a much lower temperature, $T = 20$ K, by Cunsolo *et al* [60]. In both cases, an x-ray diffraction measurement was also carried out in parallel, which showed substantially similar results, but much lower error bars. In both cases, the x-ray experimental data reported a main peak of $S(Q)$ markedly lower than 2 and consistent with their PIMC simulation results. The same technique was also used to measure $S(Q)$ for liquid deuterium [60] which, again, turned out to be in good agreement with their PIMC simulations. Thus, even though the x-ray results are not directly comparable with the neutron data, due to different thermodynamic conditions, the positive comparison with the PIMC simulations indirectly supports the neutron diffraction results.

8. Discussion and conclusions

The atom–atom structure factor of the hydrogen liquids has been determined using neutron diffraction techniques. For a simple liquid, this is the main structural information that can be experimentally accessed at the microscopic level. Using a reliable model for the intramolecular structure, this information can be deconvoluted and the structural information on the COM distribution can be derived. In both cases, the TOF diffraction experiment, carried out at small scattering angles, represented the pioneering experiment. However, a further experimental investigation, using a two-axis classic diffractometer, was necessary, in both cases, to improve the quality of the data. The experimental results for the two isotopes are characterized by a different structure factor which, in turn, calls for a different microscopic distribution of the molecular COMs, even for corresponding thermodynamic points (i.e. liquid phase close to the triple point). This main result is depicted in figure 3. As we may assume that hydrogen and deuterium experience, to a first approximation, the same intermolecular potential, this difference must be entirely attributed to the mass difference of the two isotopes and, hence, to the different size of the relative quantum effects that are dependent on mass (cf equation (1)). The higher main peak in the $S(Q)$ of liquid deuterium calls for a more extended structure, in space, around each molecular COM. In other words, the structural features of the radial distribution function, in liquid deuterium, are expected to extended farther that the corresponding ones in hydrogen. This is what should be expected on the basis of a smaller zero-point motion of the deuterium molecule with respect to that of hydrogen.

From a comparison between the deuterium and hydrogen structural data, a different *scale factor* emerges. This suggests a larger effective size of the hydrogen molecule with respect to deuterium. Again, this appears as a typical quantum effect bound to the lower mass and to the consequent larger spatial width of the single-particle wavepacket. It is important to stress that this *scale factor* appears as a common characteristic of many different features (i.e. the structure factor and its thermodynamic derivatives) that were measured on different instruments and using different neutron diffraction techniques.

The experimental information has been compared with the available quantum mechanical simulation results for the structure factors and their thermodynamic derivatives. While for the heavier isotope a very good agreement is always found, the situation appears less definite for the lighter isotope, probably due to the more difficult analysis of the hydrogen experiment. In the case of deuterium, the comparison between the PIMC results and the experiment is extremely positive, both for the structure factor and for its thermodynamic derivatives (cf figures 4 and 5, as well as figure 1 of [44]). However, this picture appears less optimistic for hydrogen. A possible residual systematic error seems to affect both the experimental data sets of hydrogen, as in the upper part of figure 4. By contrast, the simulation results average the two experimental behaviours. In addition, from a comparison between experiment and simulation, a clear slight variance still appears in the scale factor of the hydrogen data (cf figures 4 and 5). This

occurrence seems to be confirmed by the fact that two different experiments suggest the same behaviour (cf figure 4, upper part). Unfortunately, the present accuracy of the hydrogen data does not allow us to interpret this fact as a clear suggestion for a different intermolecular potential of the two isotopes. However, it is a fact that the NWB intermolecular potential is strongly based on the scattering data of deuterium. Finally, it should be stressed once more that the hydrogen neutron diffraction experiment is so difficult, and the error bars so large, that any definite conclusion is impossible at the moment.

A few comments should be made on the discussion of figure 6. Here, the PIMC data are compared with two different neutron scattering determinations of the microscopic structure factor. In our case, $S(Q)$ results from a diffraction experiment, while the other determination was obtained by integrating the measured inelastic spectra. The two experiments give rather different results, with our determination closer to the PIMC simulation results. Apart from the obvious preference for our own data, we also have indirect confirmation in favour of this choice from another, independent, recent experimental result that was obtained using x-ray scattering. In this case, the thermodynamic points are dissimilar and therefore it is impossible to draw all the data on the same figure. However, the observed agreement of the x-ray data of [59] and [60] with their PIMC results seems to confirm our findings indirectly, and the simulation data are not too far from the real behaviour of liquid hydrogen.

To conclude, we have shown that, using neutron diffraction, a reliable determination of the microscopic structure factor of liquid hydrogen is possible. The hydrogen results are qualitatively similar, but not quantitatively, to those of deuterium, and the difference between the two is mainly assigned to the different quantum behaviour of the two isotopes. This is ascribed to a larger zero-point motion of the hydrogen molecular COM. The occurrence of quantum effects also determines the observed increase in the effective molecular diameter of the hydrogen molecule with respect to deuterium. This is interpreted as a different broadening of the particle wavefunction which is driven by a different molecular mass.

Acknowledgments

The author wishes to thank his close collaborators, F Barocchi, U Bafile, M Celli, D Colognesi, F Formisano, E Guarini and R Magli, who have contributed, with their expertise and skill, to the many experiments and their interpretation. Particular thanks are due to M Neumann who developed the PIMC code, so extensively used in the interpretation of the experimental data. Last but not least, the skilful assistance of the instrument scientists and technical staff of ISIS and ILL is gratefully acknowledged. Most of the experimental work described in this review has been made possible by the International Cooperation Agreement between CNR (Italy) and ISIS and that between INFM (Italy) and ILL.

References

[1] Dewar J 1927 *Collected Papers of Sir James Dewar* ed Lady Dewar (Cambridge: Cambridge University Press)
[2] Mecke R 1925 *Z. Phys.* **31** 709
[3] Heisenberg W 1926 *Z. Phys.* **33** 879
Heisenberg W 1926 *Z. Phys.* **39** 499
[4] Urey H C, Brickwedee F G and Murphy G M 1932 *Phys. Rev.* **40** 1
[5] Oliphant M L E, Harteck P and Rutherford E 1934 *Proc. R. Soc.* A **144** 692
[6] Alvarez L W and Cornog R 1940 *Phys. Rev.* **57** 248
[7] Faltings F and Harteck P 1950 *Z. Naturf.* A **5** 438
[8] Grosse A V, Johnston L, Wolfgang R L and Libby W F 1951 *Science* **113** 1
[9] Silvera I F 1980 *Rev. Mod. Phys.* **52** 393

[10] Roder H M, Childs G E, McCarty R D and Angerhofer P E 1973 *Survey of the Properties of the Hydrogen Isotopes below their Critical Temperatures* NBS Technical Note No 641
[11] Balucani U and Zoppi M 1994 *Dynamics of the Liquid State* (Oxford: Oxford University Press)
[12] Hansen J P and McDonald I 1986 *Theory of Simple Liquids* (London: Academic)
[13] Hildebrand R H and Nagle D E 1953 *Phys. Rev.* **92** 517
[14] Wood J G 1954 *Phys. Rev.* **94** 731
[15] http://www.sns.gov/aboutsns/source.htm
[16] Schlapbach L and Züttel A 2001 *Nature* **414** 353
[17] Furikawa K 1962 *Rep. Prog. Phys.* **25** 395
[18] Frisch H L and Salsburg Z W 1968 *Simple Dense Fluids* (New York: Academic)
[19] Yarnell J L, Katz M J, Wenzel R G and Koenig S H 1973 *Phys. Rev.* A **7** 2130
[20] Sköld K and Price D L (eds) 1986 *Neutron Scattering* (Orlando, FL: Academic)
[21] Egelstaff P A 1992 *An Introduction to the Liquid State* (Oxford: Clarendon)
[22] Andreani C, Dore J C and Ricci F P 1991 *Rep. Prog. Phys.* **54** 731
[23] Placzek G 1952 *Phys. Rev.* **86** 377
[24] Fermi E 1936 *Ric. Sci.* **7** 13
[25] Squires G L 1996 *Introduction to the Theory of Thermal Neutron Scattering* (New York: Dover)
[26] Lovesey S W 1986 *Theory of Neutron Scattering from Condensed Matter* vol 1 (Oxford: Oxford University Press)
[27] Zoppi M, Magli R, Howells W S and Soper A K 1989 *Phys. Rev.* A **39** 4684
[28] Zoppi M 1991 *Physica* B **168** 177
[29] Benmore C J and Soper A K 1998 The SANDALS manual *Rutherford Laboratory Technical Report* RAL-TR-98006
[30] Zoppi M, Bafile U, Magli R and Soper A K 1993 *Phys. Rev.* E **48** 1000
[31] Zoppi M, Soper A K, Magli R, Barocchi F, Bafile U and Ashcroft N W 1996 *Phys. Rev.* E **54** 2773
[32] Van Kranendonk J 1983 *Solid Hydrogen* (New York: Plenum)
[33] Egelstaff P A, Page D I and Powles J G 1971 *Mol. Phys.* **20** 881
[34] Sears V F 1966 *Can. J. Phys.* **44** 1279
[35] Talhouk S J, Harris P M, White D and Erickson R A 1968 *J. Chem. Phys.* **48** 1273
[36] Ishmahev S N, Sadikov I P, Chernyshov A A, Isakov S L, Vindryaevsky B A, Kobelyev G V, Sukhoparov V A and Telepnev A S 1988 *Sov. Phys.–JETP* **7** 190
[37] Allen M P and Tildesley D J 1987 *Computer Simulation of Liquids* (Oxford: Oxford University Press)
[38] Neumann M and Zoppi M 1991 *Phys. Rev.* A **44** 2474
[39] Ceperley D M 1995 *Rev. Mod. Phys.* **67** 279
[40] Young J A and Koppel J U 1964 *Phys. Rev.* A **33** 603
[41] Zoppi M 1993 *Physica* B **183** 235
[42] Guarini E, Barocchi F, Magli R, Bafile U and Bellissent-Funel M C 1995 *J. Phys.: Condens. Matter* **7** 5777
[43] Bafile U, Barocchi F, Guarini E, Magli R and Zoppi M 1995 *Physica* B **213/214** 465
[44] Zoppi M, Bafile U, Guarini E, Barocchi F, Magli R and Neumann M 1995 *Phys. Rev. Lett.* **75** 1779
[45] Zoppi M, Celli M and Soper A K 1998 *Phys. Rev.* B **58** 11905
[46] Celli M, Rhodes N, Soper A K and Zoppi M 1999 *J. Phys.: Condens. Matter* **11** 10229
[47] Langel W, Price D L, Simmons R O and Sokol P E 1988 *Phys. Rev.* B **38** 11275
[48] Herwig K W, Sokol P E, Sosnick T R, Snow W M and Blasdell R C 1990 *Phys. Rev.* B **41** 103
[49] Celli M, Colognesi D and Zoppi M 2000 *Eur. J. Phys.* B **14** 239
[50] Zoppi M, Colognesi D and Celli M 2001 *Eur. J. Phys.* B **23** 171
[51] Zoppi M, Bafile U, Celli M, Cuello G J, Formisano F, Guarini E, Magli R and Neumann M 2003 *J. Phys.: Condens. Matter* **15** S107
[52] Norman M J, Watts R O and Buck U 1984 *J. Chem. Phys.* **81** 3500
[53] Zoppi M, Neumann M and Celli M 2002 *Phys. Rev.* B **65** 92204
[54] Silvera I F and Goldman V V 1978 *J. Chem. Phys.* **69** 4209
[55] Verlet L 1968 *Phys. Rev.* **165** 201
[56] Bermejo F J, Kinugawa K, Cabrillo C, Bennington S M, Fåk B, Fernández-Díaz M T, Verkerk P, Dawidowski J and Fernández-Perea R 2000 *Phys. Rev. Lett.* **84** 5359
[57] Hansen J P and Verlet L 1969 *Phys. Rev.* **184** 151
[58] Zoppi M, Celli M, Bafile U, Guarini E and Neumann M 2001 *Condens. Matter News* **4** 283
[59] Pratesi G, Colognesi D, Cunsolo A, Verbeni R, Nardone M, Ruocco G and Sette F 2002 *Philos. Mag.* B **82** 305
[60] Cunsolo A, Pratesi G, Colognesi D, Verbeni R, Sampoli M, Sette F, Ruocco G, Senesi R, Krisch M H and Nardone M 2002 *J. Low Temp. Phys.* **129** 117